Sparsity based full rank polarimetric reconstruction of coherence matrix T

H. Aghababaee, G. Ferraioli, Laurent Ferro-Famil, G. Schirinzi, Yue Huang

remote sensing

MDPI

Article

Sparsity Based Full Rank Polarimetric Reconstruction of Coherence Matrix T

Hossein Aghababaee [1,*], Giampaolo Ferraioli [1], Laurent Ferro-Famil [2], Gilda Schirinzi [1] and Yue Huang [2]

[1] Università degli Studi di Napoli "Parthenope", 80133 Napoli NA, Italy; giampaolo.ferraioli@uniparthenope.it (G.F.); gilda.schirinzi@uniparthenope.it (G.S.)
[2] Institut d'Électronique et de Télécommunications de Rennes 1, F-35042 Rennes, Frances; laurent.ferro-famil@univ-rennes1.fr (L.F.-F.); yue.huang@univ-rennes1.fr (Y.H.)
* Correspondence: aghababaee@uniparthenope.it

Received: 27 February 2019; Accepted: 28 May 2019; Published: 30 May 2019

Abstract: In the frame of polarimetric synthetic aperture radar (SAR) tomography, full-ranks reconstruction framework has been recognized as a significant technique for fully characterization of superimposed scatterers in a resolution cell. The technique, mainly is characterized by the advantages of polarimetric scattering pattern reconstruction, allows physical feature extraction of the scatterers. In this paper, to overcome the limitations of conventional full-rank tomographic techniques in natural environments, a polarimetric estimator with advantages of super-resolution imaging is proposed. Under the frame of compressive sensing (CS) and sparsity based reconstruction, the profile of second order polarimetric coherence matrix **T** is recovered. Once the polarimetric coherence matrices of the scatterers are available, the physical features can be extracted using classical polarimetric processing techniques. The objective of this study is to evaluate the performance of the proposed full-rank polarimetric reconstruction by means of conventional three-component decomposition of **T**, and focusing on the consistency of vertical resolution and polarimetric scattering pattern of the scatterers. The outcomes from simulated and two different real data sets confirm that significant improvement can be achieved in the reconstruction quality with respect to conventional approaches.

Keywords: full-rank polarimetric SAR tomography; sparsity based reconstruction; three-component decomposition; forest

1. Introduction

Extraction of physical features of forest structure is important in the monitoring and modeling of the dynamics of the ecosystem. Synthetic aperture radar (SAR) tomography (TomoSAR) with resolution capability in the elevation directions is a multi-dimensional signal processing technique that has great value for the estimation of forest structures [1,2]. Generally, forest environment is considered as two-layer media along the height dimension, in which the medium is characterized by random distributed volumetric scattering over the ground [3]. Although, SAR tomography is a natural solution for the vertical structure reconstruction of such an environment, but fails to interpret and characterize the specification of the targets presented in the media. With the aim of forest structure characterization, polarimetric SAR tomography (PolTomoSAR) is a useful tool for fully interpretation of electromagnetic behavior of the illuminated objects [4,5]. The method consists in full-rank reconstruction of the power spectrum and polarimetric scattering pattern of superimposed scatterers, allowing physical feature extraction from the forest structures. Full-rank polarimetric SAR tomography techniques are hence of the great interest.

Full-rank reconstruction techniques, including conventional Beamforming and Capon have been introduced and successfully applied to characterize the forest environment and under-Foliage objects using polarimetric multi-baseline (MB) data sets [4,5]. Despite the undeniable improvement in scene characterization by the conventional employed methods, some quality problems in the reconstruction accuracy of those methods may be raised due to the uneven acquisition sampling or infrequent passes over the scene of interest. Moreover, the limited extension of the tomographic aperture imposes an additional criticality in the achievable desirable resolution by the classical approaches.

In the frame of sparse based reconstruction technique, i.e., compressive sensing (CS) [6,7], recent studies have been addressed the typical TomoSAR inversion problem [8–11]. The method aims at reconstruction of the vertical power spectrum of the superimposed scatterers under the condition that the reflectivity signal is sparse along the height dimension. As it has been demonstrated in [12], the most important peculiarity of sparse based retrieval is super-resolution achievement with even a reduced number of irregular passes. In which, the sparse based reconstruction is able to identify the superimposed scatterers whose distance is lower than the vertical Rayleigh resolution. In particular to forest environment, the sparse representation of distributed media in the elevation dimension is exploited in the wavelet domain [12,13]. Moreover, to the aim of further discrimination, the studies in [13,14], extended this method to the polarimetric reflectivity (i.e., span image) of the observed scene by means of polarimetric multi-baseline data. Reference [10] provides another view and processing strategy to reconstruct the vertical structure of forested areas using the sparsity based estimator. The method is tailored to validate the sparseness and compressible of canopy backscattering in wavelet domain by separation of the ground contribution using the algebraic decomposition technique introduced in [15]. From the fact that the wavelet is able to sparsify the smooth backscattering from the canopy, while the point like scatterers from the ground might be spread out over the wavelet domain, reference [16] employed the hybrid basis that lets to discrete and sparsify the ground and canopy's contributions in the object and wavelet domains, respectively.

In general, although, the performance of sparse based reflectivity reconstruction has been assessed and appreciated, but full-rank simultaneously reconstruction of the power spectrum and polarimetric scattering pattern can be more efficient. Differently from such a polarimetric reflectivity reconstruction technique by compressive sensing in [13], where the polarization was employed to improve the synthesizing performance and the discrimination between vertically aligned scatterers, this paper aims at presenting a full rank reconstruction framework based on the hybrid sparse representation of polarimetric information in order to fully characterize the objects under analysis. The framework is able to recover full information of the scatterers from a reduced set of measurements and achieve to the super-resolution capability [13]. In particular, the method works with second order statistics of polarimetric MB SAR data set, and exploits sparse representation of polarimetric information to recover the polarimetric coherence matrix $\mathbf{T}$ of the superimposed scatterers situated at different height levels. In this way, the polarimetric MB covariance fitting methodology from compressive sensing perspective is exploited to retrieve the tomogram of the polarimetric coherence matrix. Availability of coherence matrix tomogram allows employing of all the classical polarimetric processing techniques including three-component Freeman-Durden decomposition technique [17] with the aim of physical features extraction and scene investigation.

This paper begins with an overview of the polarimetric SAR signal model as well as the basic principles of full-rank TomoSAR focusing using conventional approaches in Section 2. The proposed sparsity based full-rank reconstruction is given in Section 3. Numerical examples of comparative analyses on the effectiveness of the proposed method with respect to conventional approaches are given in Section 4. Experimental results using two real data sets acquired by the European Space Agency's campaigns TropiSAR and AfriSAR are provided in Section 5. Further discussion and conclusion on the reported results are then given in Sections 6 and 7.

2. Polarimetric SAR Tomography

2.1. SAR Tomography Signal Model

Let us refer to an azimuth-range resolution cell that consists of M superimposed scatterers along the elevation dimension, then the stack data vector measured by a multi-baseline configuration over N SAR acquisitions $\mathbf{y} \in \mathbb{C}^{N\times 1}$, can be represented by:

$$\mathbf{y}(l) = \sum_{i=1}^{M} s_i(l)\mathbf{a}(z_i) + \mathbf{n}(l) = \mathbf{A}(\mathbf{z})\mathbf{s}(l) + \mathbf{n}(l) \tag{1}$$

where $\mathbf{s}(l) \in \mathbb{C}^{M\times 1}$ is the source signal vector with l realizations of the signal acquisition contains the M complex backscatterings, and $\mathbf{A} = [\mathbf{a}(z_1) \ldots \mathbf{a}(z_M)]$ indicating steering matrix contains M steering vectors, and $\mathbf{n}$ is the complex additive noise.

Using a fully polarimetric TomSAR configuration with 3 polarimetric channels, *f.i.* in Pauli vector representation, the received signal $\mathbf{y}_p(l) = [\mathbf{y}_1(l)^{\mathrm{T}}\ \mathbf{y}_2(l)^{\mathrm{T}}\ \mathbf{y}_3(l)^{\mathrm{T}}]^{\mathrm{T}} \in \mathbb{C}^{3N\times 1}$ that is formed by the response of each stack of polarization can be represented by:

$$\mathbf{y}_{\mathrm{p}}(l) = \sum_{i=1}^{M} s_i(l)\mathbf{a}(z_i, \mathbf{k}_i) + \mathbf{n}(l) = \mathbf{A}(\mathbf{z}, \mathbf{K})\mathbf{s}(l) + \mathbf{n}(l) \tag{2}$$

where $\mathbf{a}(z_i,\mathbf{k}_i)=(\mathbf{I}_{(3\times 3)}\otimes\mathbf{a}(z_i))\mathbf{k}_i=\mathbf{B}_{\mathbf{a}}(z_i)\mathbf{k}_i$ represents the polarimetric steering vector, in which $\mathbf{k_i}$ is the polarimetric target scattering vector, $\mathbf{I}_{(3\times 3)}$ is a 3×3 identity matrix, and $\otimes$ denotes the Kronecker product. The complex additive noise $\mathbf{n}$ is assumed to follow a Gaussian distribution with zero mean and standard deviation of ${\sigma_n}^2$. Then, the covariance matrix of observed polarimetric signal (2) is generally given by:

$$\mathbf{R}_p = E\left\{\mathbf{y}_{\mathrm{p}}(l)\mathbf{y}_{\mathrm{p}}(l)^{\dagger}\right\} = \sum_{i=1}^{M} \mathbf{T}(z_i) \otimes \mathbf{a}(z_i)\mathbf{a}(z_i)^{\dagger} + \sigma_n^2\mathbf{I} \tag{3}$$

where E is the expectation operator. The second order polarimetric information is described by the semi positive definite coherency matrix of the considered scatterer, i.e., $\mathrm{E}\{|s_i(l)|^2\ \mathbf{k}_i\mathbf{k}_i\dagger\} = \mathbf{T}(zi) \in \mathbb{C}^{3\times 3}$.

Full-rank inversion framework is involved in the reconstruction of the coherence matrix of the superimposed scatterers allowing fully characterizing of them. Concerning to the distributed environments, in what follows, the two most competitive classical techniques are reviewed.

2.2. Classical Full-Rank Focusing Techniques

With the aim of full-rank reconstruction from distributed environment, the polarimetric inversion of conventional Beamforming and Capon were represented in [4,18,19]. As the case of single polarimetric, full-rank Beamforming is robust to the artifacts, but limited by coarse resolution. The data adaptive full-rank Capon for high signal-to-noise ratio (SNR) can achieve to improved resolution and enjoys side-lobe suppression capability. By referring to [4,18], the solution of these full-rank polarimetric reconstruction methods can be expressed as:

$$\begin{array}{ll} \text{Beamforming} & \mathbf{T}(z_i) = \mathbf{B}_{\mathbf{a}}^{\dagger}(z_i)\,\hat{\mathbf{R}}_p\,\mathbf{B}_{\mathbf{a}}(z_i) \\ \text{Capon} & \mathbf{T}(z_i) = \left(\mathbf{B}_{\mathbf{a}}^{\dagger}(z_i)\,\hat{\mathbf{R}}_p^{-1}\,\mathbf{B}_{\mathbf{a}}(z_i)\right)^{-1} \end{array} \tag{4}$$

where $\hat{\mathbf{R}}_p$ is the polarimetric MB sample covariance matrix estimated over the L independent and identically distributed samples, i.e., $\hat{\mathbf{R}}_p = \sum_{l}^{L} \mathbf{y}_p(l)\mathbf{y}_p(l)^{\dagger}/L$.

3. Hybrid Sparse Based Full-Rank Reconstruction

The proposed hybrid sparsity based full-rank reconstruction involves in the L1-norm minimization between the observed and modeled data covariance matrices as follows.

$$\min_{\mathbf{x}} \left\|\mathbf{x}\right\|_1 , \quad \text{subject to} \quad \left\| \mathbf{R_p} - \hat{\mathbf{R}}_\mathbf{p} \right\|_2 \leq \varepsilon \tag{5}$$

where $\mathbf{R}_p \in \mathbb{C}^{3N\times 3N}$ is the modeled polarimetric MB covariance matrix that is represented in the Equation (7), ε is an upper bound on the noise level, and $\mathbf{x} \in \mathbb{C}^{9M\times 1}$ is a stack vector contains the coherence matrix ($\mathbf{T}$) entries of M uncorrelated superimposed scatterers in a hybrid sparse domain, i.e.,

$$\mathbf{x} = vec\left\{ (\mathbf{I}_{(3\times 3)} \otimes \mathbf{H}) \underbrace{\begin{bmatrix} \mathbf{T}_{11}(\mathbf{z}) & \mathbf{T}_{12}(\mathbf{z}) & \mathbf{T}_{13}(\mathbf{z}) \\ \mathbf{T}_{21}(\mathbf{z}) & \mathbf{T}_{22}(\mathbf{z}) & \mathbf{T}_{23}(\mathbf{z}) \\ \mathbf{T}_{31}(\mathbf{z}) & \mathbf{T}_{32}(\mathbf{z}) & \mathbf{T}_{33}(\mathbf{z}) \end{bmatrix}}_{\mathbf{T}(\mathbf{z})} \right\} = \begin{bmatrix} \mathbf{HT}_{11}(\mathbf{z}) \\ \mathbf{HT}_{21}(\mathbf{z}) \\ \mathbf{HT}_{31}(\mathbf{z}) \\ \vdots \\ \mathbf{HT}_{33}(\mathbf{z}) \end{bmatrix} \tag{6}$$

$$\mathbf{H} = \begin{bmatrix} \mathbf{I}_{(Mg\times Mg)} & \mathbf{0} \\ \mathbf{0} & \boldsymbol{\psi}_{(Mv\times Mv)} \end{bmatrix}$$

where $\mathbf{T}(\mathbf{z}) \in \mathbb{C}^{3M\times 3}$ stands for the vertical polarimetric coherence matrix of all the possible heights, in which each $\mathbf{T}_{ij}(\mathbf{z})$ is a $M\times 1$ vector. In addition, $vec\{.\}$ is the vectorization operator and $\mathbf{H}$ is the considered hybrid sparsifying basis. It should be noted that $\mathbf{I_{(Mg\times Mg)}}$ in $\mathbf{H}$ is set to an identity matrix in order to cover the fact that the Mg ground backscatterings are sparse in the object domain, while the wavelet transform operator $\boldsymbol{\psi}$ sparsifies the above ground distributed backscatterings from the canopy. Within the range of height of ambiguity and taking a window with width of Δ, the intervals ($z_1, \ldots .z_g+\Delta$) with length of Mg and ($z_g+\Delta, \ldots ..,z_M$) with length of $M_v = M-M_g$ indicate the object and wavelet domain intervals, respectively; whereas z_g is *a priori* known ground height that can be estimated using the techniques introduced in [15,20] or from the external source of information. Finally, the modeled polarimetric MB covariance matrix $\mathbf{R}_p$ in Equation (5) is represented by:

$$\mathbf{R}_p = (\mathbf{I}_{(3\times 3)} \otimes \mathbf{A}(\mathbf{z})) \begin{bmatrix} \mathrm{diag}(\mathbf{T}_{11}(\mathbf{z})) & \mathrm{diag}(\mathbf{T}_{12}(\mathbf{z})) & \mathrm{diag}(\mathbf{T}_{13}(\mathbf{z})) \\ \mathrm{diag}(\mathbf{T}_{21}(\mathbf{z})) & \mathrm{diag}(\mathbf{T}_{22}(\mathbf{z})) & \mathrm{diag}(\mathbf{T}_{23}(\mathbf{z})) \\ \mathrm{diag}(\mathbf{T}_{31}(\mathbf{z})) & \mathrm{diag}(\mathbf{T}_{32}(\mathbf{z})) & \mathrm{diag}(\mathbf{T}_{33}(\mathbf{z})) \end{bmatrix} (\mathbf{I}_{(3\times 3)} \otimes \mathbf{A}(\mathbf{z}))^\dagger \tag{7}$$

where diag(.) is the diagonalization operator.

In order to sufficiently sparsify the canopy backscatterings, the Symlet wavelet basis can be a good choice due to the orthogonality and their nearly symmetric specification. From the literature [10,13,16], the Symlet function with 4 vanishing moments and 3 levels of decomposition provides appropriate performance in tomographic compressive sensing of forested areas, and hence is used in this study as well. It should be noted that, in order to recover $\mathbf{T}(\mathbf{z})$, Equation (5) is transformed into the second-order cone programming formulation and solved in the field of sparse recovery estimation [10,12,16].

4. Numerical Example

The behavior of SAR backscattering from forest areas can be commonly described using the three mechanisms, including volumetric, first-order surface or single-bounce, and double-bounce scattering mechanisms. Along the vertical dimension of the scene and of course depending on the frequency of the employed wave in SAR system, the distributed volumetric scattering mechanism mainly is perceived from the canopy, while the occurrence of some odd-bounce scatterings is also feasible. Instead, due to the ground-trunk wave interaction, double bounce is mostly dominant scattering mechanism on the

ground height level, while some surface scatterings in case of direct backscattering from the ground and volume scattering when the ground is covered by small vegetation can be expected.

Correspond to the above-described forest scenario, a two-component signal with two phase centers one on the ground, and the other 5 m above it with wide angular spreading representing canopy backscattering is simulated (shown in Figure 1). The scattering patterns of ground scatterers are set to odd and double bounce mechanisms, while of the canopy is set to ensemble volumetric backscattering and some surface scatterings.

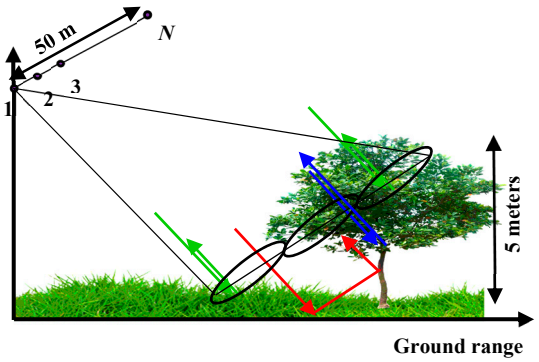

Figure 1. Simulated multi-baseline SAR geometry and the polarimetric backscatterings from forest. Red, green and blue indicate the double-bounce, volumetric and surface scattering mechanisms, respectively.

The simulated models of polarimetric coherence matrix in a simple case are given with Equation (8). In the model, odd-bounce ($\mathbf{T}_s$) follows symmetric form by the first-order Bragg surface scatterer and double-bounce ($\mathbf{T}_d$) is modeled by a dihedral corner reflector [17]. Physically the parameter β in $\mathbf{T}_s$ is the ratio of horizontal to the vertical polarized reflection coefficient from surface scattering. Moreover, the parameter α in $\mathbf{T}_d$ is the ratio of the horizontal to vertical polarized reflection coefficient of the ground multiplied by the same reflection ratio from the vegetation trunk. In addition, the volumetric scattering ($\mathbf{T}_v$) is simulated by the given diagonal matrix with parameter ρ that indicates the power of volume scattering to the surface and double-bounce scatterings [21].

Finally, by the coherent superposition of simulated ground and canopy coherence matrices using Equation (3), multi-baseline polarimetric covariance matrix is generated. It should be noted that the considered scene in Figure 1, is observed by $N = 6$ polarimetric SAR systems, whose orthogonal baselines (b_n) are evenly distributed spanning 50 m by Δkz = 0.125, where kz is the phase to height conversion parameter.

$$\begin{aligned}
\text{Odd} - \text{bounce} \qquad & \mathbf{T}_s = \frac{1}{1+|\beta|^2}\begin{bmatrix} |\beta|^2 & \beta & 0 \\ \beta^\dagger & 1 & 0 \\ 0 & 0 & 0 \end{bmatrix}, \quad |\beta| \le 1 \\
\text{Double} - \text{bounce} \qquad & \mathbf{T}_d = \frac{1}{1+|\alpha|^2}\begin{bmatrix} |\alpha|^2 & \alpha & 0 \\ \alpha^\dagger & 1 & 0 \\ 0 & 0 & 0 \end{bmatrix}, \quad |\alpha| \le 1 \\
\text{Volumetric} \qquad & \mathbf{T}_v = \frac{1}{3-\rho}\begin{bmatrix} 1+\rho & 0 & 0 \\ 0 & 1-\rho & 0 \\ 0 & 0 & 1-\rho \end{bmatrix}, \quad |\rho| \le 1
\end{aligned} \tag{8}$$

Figure 2, shows the span profile computed from the reconstructed polarimetric coherence matrix $\mathbf{T}$ using different classical methods and the proposed hybrid sparsity based technique as well. Since the two phase centers are inside the Fourier resolution, as can be seen, Beamforming is failed to identify and separate the backscatterings from ground and the canopy and consequently an interference signal is reconstructed. Capon is able to improve the vertical resolution, while hybrid sparsity based

reconstruction achieves to the desirable super-resolution and gives peaks in the right positions of the scatterers.

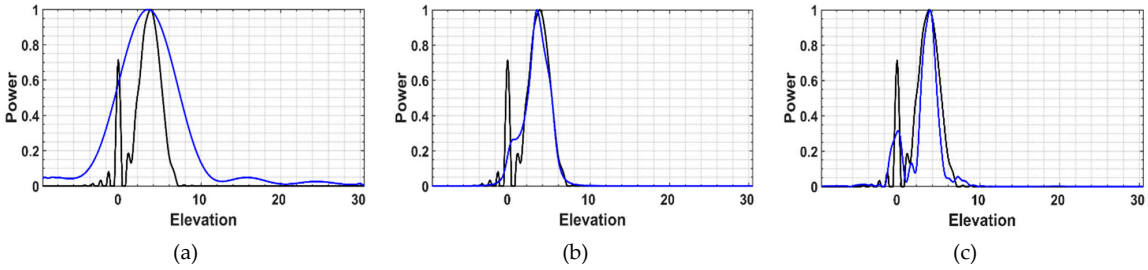

Figure 2. Extracted span profiles of the simulated scenario with full-rank reconstruction of **T**, (**a**) Beamforming, (**b**) Capon, (**c**) the proposed method. Blue and black indicate the reconstructed and simulated signals.

To evaluate the effectiveness of the methods in polarimetric information reconstruction, the feature profiles of three-component Freeman-Durden decomposition [17] of the reconstructed **T** are extracted and represented in Figure 3. In addition to the resolution limitation, Beamforming is not able to identify the double-bounce scattering from the ground, in which only volumetric and surface scatterings are reconstructed. Although, Capon is able to identify the scattering mechanisms of the ground and canopy, but it may suffer from the resolution problem. However, it can be verified that the most similar profiles to the original one are produced by the proposed method in Figure 3d, in which the resolution limitation is resolved and scattering patterns are well identified.

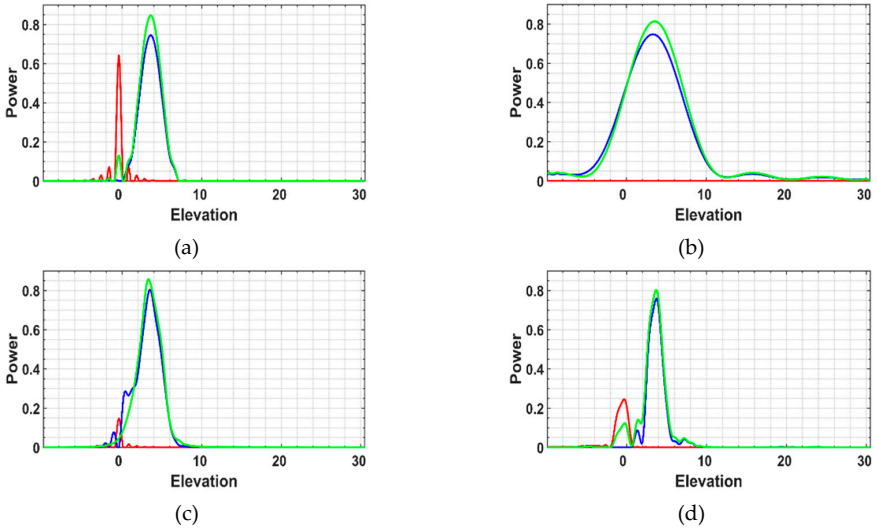

Figure 3. Extracted features from three-component decomposition of reconstructed **T**. (**a**) simulated, (**b**) Beamforming, (**c**) Capon, and (**d**) proposed method. Red, green and blue indicate the profiles of double bounce, volumetric and surface scattering mechanisms.

5. Experimental Results

In analogy to the simulated experiments, full-rank reconstruction of coherence matrix, and consequently the physical features extraction using two different real data sets are proceeded with the proposed and conventional methods. The first data set is a MB stack of six fully polarimetric P-band SAR images (Figure 4a) over the forest stand of Paracou, French Guiana. The images were acquired by the ONERA SETHI airborne system on 24 August 2009, in the framework of the European Space Agency's campaign TropiSAR [22]. The flight lines were in a vertical plane, with specified shifts of 15, 30, 45, 60, and 75 m, to the reference flight line, leading the Fourier resolution about 24 m along

the elevation direction [22]. The second polarimetric TomoSAR stack is obtained in the frame of the AfriSAR campaign [23], which was carried out in Mondah, Gabon, in 2015 (Figure 4b). The stack consists of $N = 8$ polarimetric P-band images with vertical baselines of −80, −60, −20, 0, +10, +40, +60, +80 m, resulting vertical Rayleigh resolution of about 10 m to 15 m. The main objective of both airborne campaigns was biomass study in tropical forested areas, and in support of the near future long-wavelength spaceborne missions. Finally, the Pauli color composite master images of the data sets are shown in Figure 4.

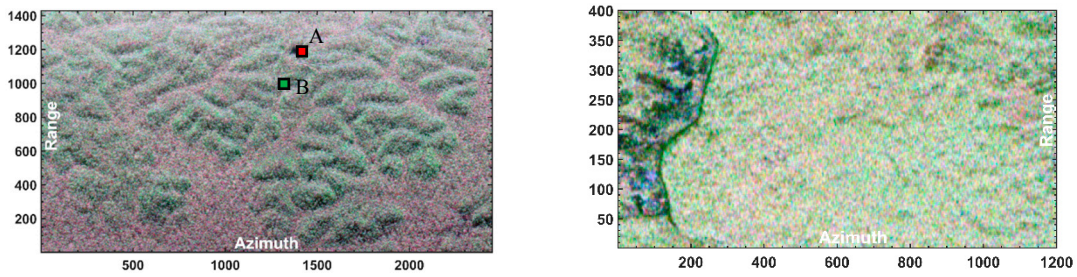

(a) TropiSAR data set (b) AfriSAR data set

Figure 4. Pauli false color composite of master images of (**a**) TropiSAR and (**b**) AfriSAR data campaigns. Point A (ground pixel) and point B (forest pixel) are two analyzed cells.

For detailed analyses on the efficiency of the proposed framework in polarimetric scattering pattern recovering, the full-rank reconstruction for two ground and forest pixels (shown in Figure 4a) is implemented and the reconstructed span and Freeman-Durden profiles are presented in Figure 5, Figure 6, Figure 7. For both cells, the phase centers from the plots are correspond to the actual ground and forest height extracted from LIDAR based measurements. In all cases, the reconstructed **T** using all employed techniques is normalized to the maximum norm of the coherence matrix along the height and then the decomposition features (red: double-bounce, green: volumetric and blue: surface scattering) are computed.

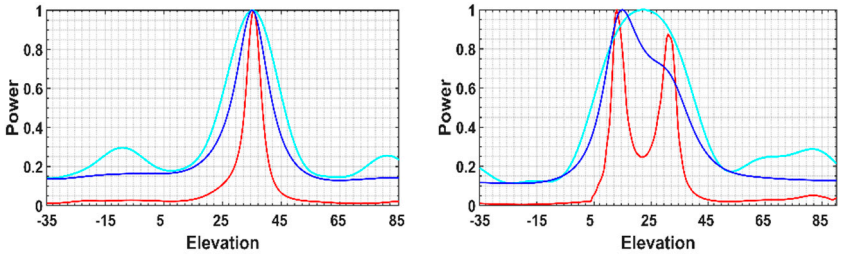

(a) (b)

Figure 5. Span profiles of ground (**a**) and forest (**b**) pixels. Cyan, blue, and red are indicative of Beamforming, Capon, and the proposed method, respectively.

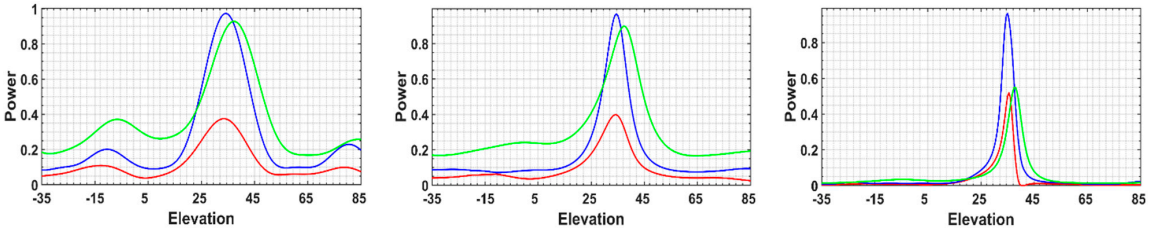

(a) (b) (c)

Figure 6. Extracted three-component features of ground pixel (shown in Figure 4a) from reconstructed **T** using (**a**) Beamforming, (**b**) Capon, and (**c**) the proposed method. Red, green and blue indicate the double-bounce, volumetric and surface scattering mechanisms.

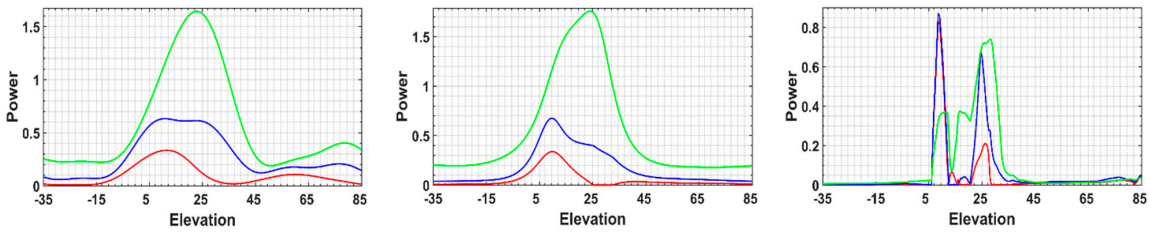

Figure 7. Extracted three-component features of forest pixel (shown in Figure 4a) from reconstructed **T** using (**a**) Beamforming, (**b**) Capon, (**c**) and the proposed method. Red, green and blue indicate the double-bounce, volumetric and surface scattering mechanisms.

Further experiments with TropiSAR data are reported in Figure 8, by Freeman-Durden tomogram reconstruction along two specified transect lines (a fixed azimuth line x = 1400 and a fixed range line r = 1000). The color-coded tomograms are generated by three features of Freeman-Durden decomposition where double-bounce, volumetric and surface scatterings are set as red, green and blue channels, respectively.

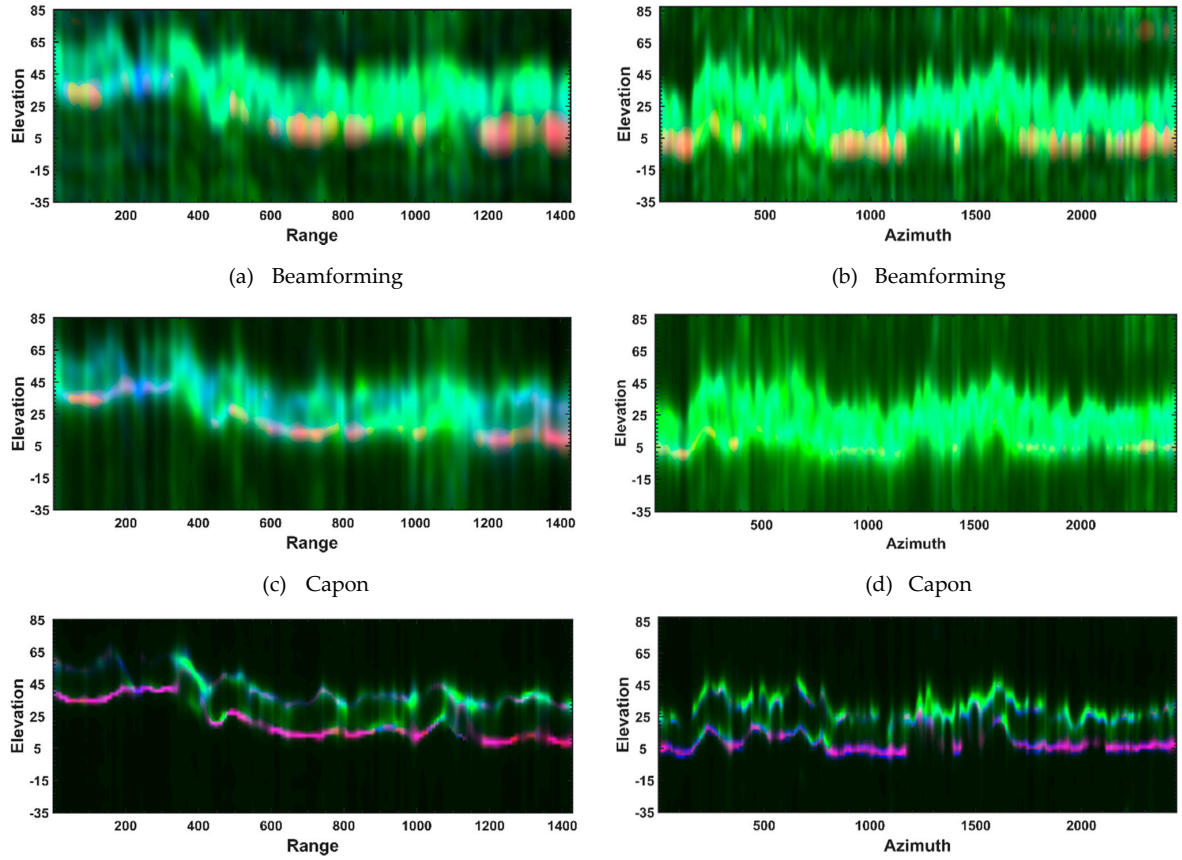

Figure 8. The color-coded Freeman-Durden tomograms of TropiSAR data set along a fixed azimuth line (**left**) and a fixed range line (**right**).

In addition, the experiments are extended to AfriSAR data set by reconstruction of the Freeman-Durden tomograms again along two different azimuth (x = 150) and range (r = 500) lines. The reconstructed tomograms of AfriSAR data are reported in Figure 9. Finally, on the basis of the experimental results, some observations are in order that discussed in the next section.

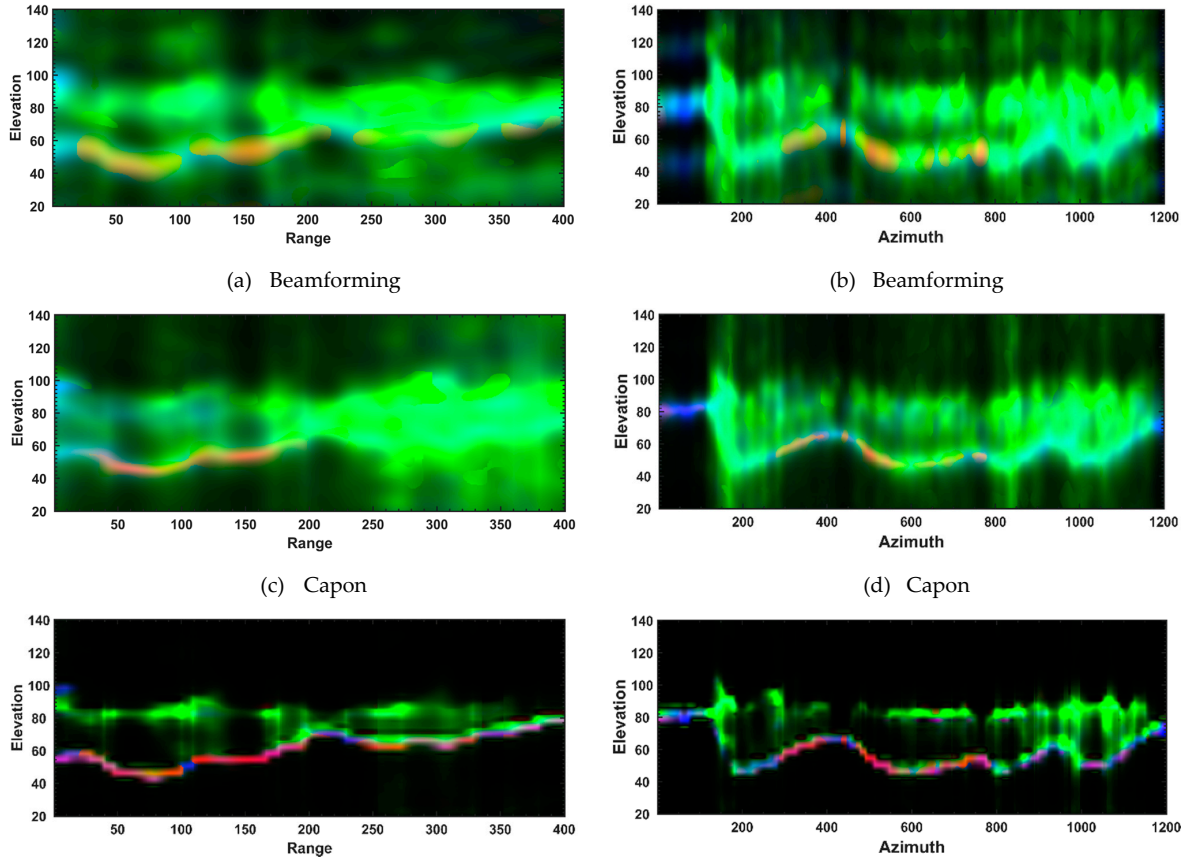

Figure 9. The color-coded Freeman-Durden tomograms of AfriSAR data set along a fixed azimuth line (**left**) and a fixed range line (**right**).

6. Discussion

From the reported span profiles using different methods in Figure 5, it is possible to affirm the resolution improvement by the hybrid sparse based reconstruction. In particular, for the forested pixel the proposed method (red profile in Figure 5) outperforms the other employed techniques in the terms of resolution and separation of superimposed scatterers. From the Freeman-Durden profiles of the ground pixel (see Figure 6), in all implemented methods, the surface scattering is recognized as the dominant scattering mechanism, while some volumetric scatterings also are recovered. For the ground pixel, similar results in term of feature extraction from polarimetric information are reconstructed, while the proposed method is able to reach improved resolution capability.

Moving to forest pixel (see Figure 7), it can be seen that both Beamforming and Capon identified volumetric as the dominant scattering mechanism on the ground and canopy height levels, while double-bounce scattering is characterized on the ground height level as the third dominant scattering mechanism (Figure 7a,b). From the proposed method, surface, volumetric and double-bounce as expected are well recovered. For the selected forest pixel, double-bounce and surface scattering are recognized as dominant mechanisms in the ground height level, which is more in coincidence with the forest reality due to the double-bounce wave interaction between ground and trunk. In the canopy height level, volumetric and some surface scattering are the main backscattering mechanisms (Figure 7c).

The given plot reveals important aspect of proposed full-rank reconstruction, in which due to the super-resolution capability the technique is able to distinguish the scatterers and properly characterize the backscattering mechanisms, while those can be interfered with existing classical approaches. Generally, resolution limitation of conventional approaches affected the reconstructed

polarimetric information, in which the backscattering mechanism of canopy is mainly characterized along the all-feasible heights. In this case, the ground backscattering due the unresolved interference is affected by the canopy backscattering and double-bounce scattering was not properly identified by such conventional approaches. However, it can be verified that the hybrid sparse based reconstruction properly identified the backscattering mechanisms along the height of ambiguity by improving the resolution capability.

From the generated color-coded Freeman-Durden tomograms using TropiSAR data in Figure 8, the resolution improvement by the sparse based reconstruction (Figure 8e,f) is again evident in comparison with the results by Beamforming (Figure 8a,b) and Capon (Figure 8c,d). Such a resolution improvements can also be verified using the reported results of AfriSAR data sets in Figure 9. In both data set, while the proposed method enjoys side-lobe suppression and produces more focused signals, results by Capon and particularly Beamforming are defocused and affected by the side-lobes. From the qualitative comparison of the reported tomograms, it can be noticed that commonly ground is identified by double-bounce scattering mechanisms in all cases. However, spread and overestimated volumetric scattering in the results by Capon and Beamforming limited ground identification. This is mostly related to the previously mentioned resolution issue and produced interference signal using standard techniques. In contrary, as it is apparent, beside the resolution improvement, ground and canopy are mainly identified by the expected double-bounces and volumetric scattering using the employed proposed method.

However, it should be pointed out that the improvement by proposed method obtained at the cost of processing time. The total running time for the proposed method in case of AfriSAR tomograms generation using a desktop PC with a 7-core processor was around 118 and 95 times more than Beamforming and Capon based reconstructions, respectively.

7. Conclusions

This study addressed the full-rank reconstruction problem for forested scenario using sparse based polarimetric SAR tomography reconstruction. In the frame of compressive sensing, a hybrid based sparse estimation method is employed in order to fully characterize the superimposed scattereres by polarimetric information reconstruction. The proposed method was evaluated using simulated and two real data sets, namely TropiSAR and AfriSAR, and it was shown that the method is able to effectively reconstruct forest structure by properly recovering of the second order polarimetric coherence matrix. From the outcomes of this study, the efficiency of the method with respect to conventional full-rank approaches was shown; in particular, the proposed method inherently reconstructed the power spectrum and polarimetric information of the scatterers simultaneously for all heights in the defined observation space, allowed countering with some possible ambiguities. However, as it was mentioned before, depart from undeniable improvement reported in this study, the proposed method might be limited somehow by the processing time.

Author Contributions: Conceptualization, methodology, validation, H.A.; Validation, conceptualization, review and editing, L.F.-F., G.F., G.S. and Y.H.

Acknowledgments: The authors would like to thank the ESA Earth Observation Campaigns Data Project for providing MB TropiSAR data.

Conflicts of Interest: The authors declare no conflicts of interest.

References

1. Aghababaee, H.; Ferraioli, G.; Schirinzi, G.; Sahebi, M.R. The Role of Nonlocal Estimation in SAR Tomographic Imaging of Volumetric Media. *IEEE Geosci. Sens. Lett.* **2018**, *15*, 729–733. [CrossRef]
2. Tebaldini, S. Forest Structure Retrieval from Multi-Baseline SARs. In *Remote Sensing of Biomass - Principles and Applications*; IntechOpen: London, UK, 2012.

3. Papathanassiou, K.; Cloude, S. Single-baseline polarimetric SAR interferometry. *IEEE Trans. Geosci. Sens.* **2001**, *39*, 2352–2363. [CrossRef]
4. Ferro-Famil, L.; Huang, Y.; Reigber, A. High-Resolution SAR Tomography using full rank Polarimetric spectral estimators. In Proceedings of the 2012 IEEE International Geoscience and Remote Sensing Symposium, Munich, Germany, 22–27 July 2012.
5. Ferro-Famil, L.; Huang, Y.; Tebaldini, S. Polarimetric characterization of 3-D scenes using high-resolution and Full-Rank Polarimetric tomographic SAR focusing. In Proceedings of the 2016 IEEE International Geoscience and Remote Sensing Symposium (IGARSS), Beijing, China, 10–15 July 2016.
6. Baraniuk, R.G. Compressive sensing [Lecture Notes]. *IEEE Signal Process. Mag.* **2007**, *24*, 118–121. [CrossRef]
7. Donoho, D.L. Compressed sensing. *IEEE Trans. Inf. Theory* **2006**, *52*, 1289–1306. [CrossRef]
8. Budillon, A.; Evangelista, A.; Schirinzi, G. SAR Tomography from Sparse Samples. In Proceedings of the 2009 IEEE International Geoscience and Remote Sensing Symposium, Cape Town, South Africa, 12–17 July 2009.
9. Budillon, A.; Evangelista, A.; Schirinzi, G. Three-Dimensional SAR Focusing From Multipass Signals Using Compressive Sampling. *IEEE Trans. Geosci. Sens.* **2011**, *49*, 488–499. [CrossRef]
10. Li, X.; Liang, L.; Guo, H.; Huang, Y. Compressive Sensing for Multibaseline Polarimetric SAR Tomography of Forested Areas. *IEEE Trans. Geosci. Sens.* **2016**, *54*, 153–166. [CrossRef]
11. Zhu, X.X.; Bamler, R. Super-Resolution Power and Robustness of Compressive Sensing for Spectral Estimation With Application to Spaceborne Tomographic SAR. *IEEE Trans. Geosci. Sens.* **2012**, *50*, 247–258. [CrossRef]
12. Aguilera, E.; Nannini, M.; Reigber, A. Wavelet-Based Compressed Sensing for SAR Tomography of Forested Areas. In Proceedings of the EUSAR 2012: 9th European Conference on Synthetic Aperture Radar, Nuremberg, Germany, 23–26 April 2012.
13. Aguilera, E.; Nannini, M.; Reigber, A. Wavelet-Based Compressed Sensing for SAR Tomography of Forested Areas. *IEEE Trans. Geosci. Sens.* **2013**, *51*, 5283–5295. [CrossRef]
14. Aguilera, E.; Nannini, M.; Reigber, A. A data adaptive compressed sensing approach to polarimetric SAR tomography. In Proceedings of the 2012 IEEE International Geoscience and Remote Sensing Symposium, Munich, Germany, 22–27 July 2012.
15. Tebaldini, S. Algebraic Synthesis of Forest Scenarios From Multibaseline PolInSAR Data. *IEEE Trans. Geosci. Sens.* **2009**, *47*, 4132–4142. [CrossRef]
16. Huang, Y.; Levy-Vehel, J.; Ferro-Famil, L.; Reigber, A. Three-Dimensional Imaging of Objects Concealed Below a Forest Canopy Using SAR Tomography at L-Band and Wavelet-Based Sparse Estimation. *IEEE Geosci. Sens. Lett.* **2017**, *14*, 1454–1458. [CrossRef]
17. Freeman, A.; Durden, S. A three-component scattering model for polarimetric SAR data. *IEEE Trans. Geosci. Sens.* **1998**, *36*, 963–973. [CrossRef]
18. Huang, Y.; Ferro-Famil, L.; Reigber, A. Under-Foliage Object Imaging Using SAR Tomography and Polarimetric Spectral Estimators. *IEEE Trans. Geosci. Sens.* **2012**, *50*, 2213–2225. [CrossRef]
19. Sauer, S.; Ferro-Famil, L.; Reigber, A.; Pottier, E. Three-Dimensional Imaging and Scattering Mechanism Estimation Over Urban Scenes Using Dual-Baseline Polarimetric InSAR Observations at L-Band. *IEEE Trans. Geosci. Sens.* **2011**, *49*, 4616–4629. [CrossRef]
20. Aghababaee, H.; Sahebi, M.R. Model-Based Target Scattering Decomposition of Polarimetric SAR Tomography. *IEEE Trans. Geosci. Sens.* **2018**, *56*, 972–983. [CrossRef]
21. An, W.; Cui, Y.; Yang, J. Three-Component Model-Based Decomposition for Polarimetric SAR Data. *IEEE Trans. Geosci. Sens.* **2010**, *48*, 2732–2739.
22. Dubois-Fernandez, P.C.; Le Toan, T.; Daniel, S.; Oriot, H.; Chave, J.; Blanc, L.; Villard, L.; Davidson, M.W.J.; Petit, M. The TropiSAR Airborne Campaign in French Guiana: Objectives, Description, and Observed Temporal Behavior of the Backscatter Signal. *IEEE Trans. Geosci. Sens.* **2012**, *50*, 3228–3241. [CrossRef]
23. Technical Assistance for the Development of Airborne SAR and Geophysical Measurements during the AfriSAR Experiment. Available online: https://earth.esa.int/documents/10174/134665/AfriSAR-Final-Report (accessed on 15 December 2018).